Observation of Narrow Optical Homogeneous Linewidth and Long Nuclear Spin Lifetimes in a Prototypical [Eu(trensal)] Complex

Senthil Kumar Kuppusamy,* Evgenij Vasilenko, Weizhe Li, Jannis Hessenauer, Christina Ioannou, Olaf Fuhr, David Hunger,* and Mario Ruben*

ABSTRACT: Coherent light−matter interfaces are key elements for many quantum information processing architectures. Rare-earth ion (REI)-containing systems featuring narrow inter-configurational f −f t ransitions a re s uitable for creating such interfaces. Recently, narrow homogeneous linewid ths (Γ_h) and long nuclear spin lifetimes (T_{1spin}) associated with two Eu^{3+} complexes featuring the $^5D_0 \rightarrow {}^7F_0$ f−f transition have been reported, elucidating that REI-molecule-based coherent light−matter interfaces can be obtained. In this study, we report a homogeneous linewidth of 2.8 MHz at 4.2 K, corresponding to an optical coherence lifetime (T_{2opt}) of 114 ns (0.11 μs), associated with the $^5D_0 \rightarrow {}^7F_0$ transition of the prototypical charge neutral Eu^{3+} complex—[Eu(trensal)]. Moreover, we have observed long nuclear spin lifetimes (T_{1spin}) up to 460 ± 80 s at 4.2 K for the complex and efficient optical pumping of hyperfine levels of the $^5D_0$ ground state. The results presented in this study indicate that narrow homogeneous linewidths and long nuclear spin lifetimes could be a generic property of molecular Eu^{3+} complexes featuring the $^5D_0 \rightarrow {}^7F_0$ transition.

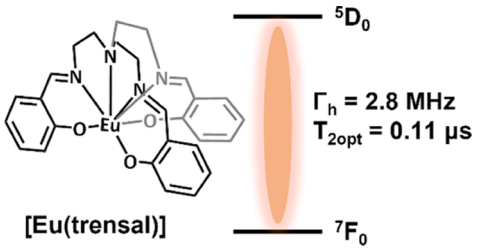

INTRODUCTION

The ever-increasing need for secure data transmission and fast information processing demands the development of novel material platforms. Consequently, platforms utilizing the quantum nature of matter have emerged to the fore, spurring a revolution under the ambit of quantum technologies or quantum information processing (QIP). A quantum property that can feature two stable states, for example, polarization of light and orientation of magnetic moment, can be used to create quantum bits (qubits),[1] provided that superposition between the states can be created. Several material platforms hosting spin qubits have been developed, and their utility to process, store, and communicate information has been demonstrated.[2] Examples include color centers in diamond,[3−5] silicon carbide,[6,7] and silicon;[8] rare-earth ion (REI) impurity centers in host lattices;[9] and magnetic[10,11] and luminescent molecules.[12] Among the platforms used, qubits based on molecules[12−18] are promising in view of their scalable nature as identical copies and the possibility of physical property tuning, following chemical synthesis protocols. Moreover, molecules can be organized in desirable ways adopting molecular self-assembly principles, facilitating programmable interqubit interactions. Consequently, spin and photonic degrees of freedom of molecules have been utilized to create superposition states. Molecules hosting spin degrees of freedom have been widely studied and are classified into three categories, namely, spin-bearing organic molecules,[19,20] transition-metal complexes,[21−29] and REI-containing complexes.[11,30−34] On the other hand, the photonic degree of freedom has been leveraged only recently to create spin−photon interfaces in transition-metal[12] and REI complexes.[35,36]

Europium (Eu^{3+}) complexes are an REI-based platform useful for QIP applications because a Eu^{3+} center[37] in a low symmetry environment can show the $^5D_0 \rightarrow {}^7F_0$ optical transition with a narrow linewidth, rendering the creation of a coherent light−matter interface. The narrow lines are inhomogeneously broadened, and the inhomogeneously broadened lines are composed of homogeneously broadened lines, indicating a subset of ions in the lattice with a narrow distribution of transition frequencies (Figure 1a). The subset of transition dipoles (ions) placed in a nearly identical environment is selectively identified using a laser whose linewidth is narrower than the homogeneous linewidth (Γ_h). From Γ_h, optical coherence lifetime (T_{2opt}) can be estimated using the relation $\Gamma_h = 1/\pi T_{2opt}$; Γ_h can be obtained from hole-burning spectroscopic studies—$\Gamma_{hole} = 2\Gamma_h$, where Γ_{hole} is the spectral holewidth. Crucially, the two stable isotopes of europium (^{151}Eu and ^{153}Eu) have nuclear spins (I = 5/2) that lead to hyperfine interactions (Figure 1b), thereby allowing the creation of hyperfine or nuclear spin qubits with long coherence lifetimes (T_{2spin}) that can be directly read out

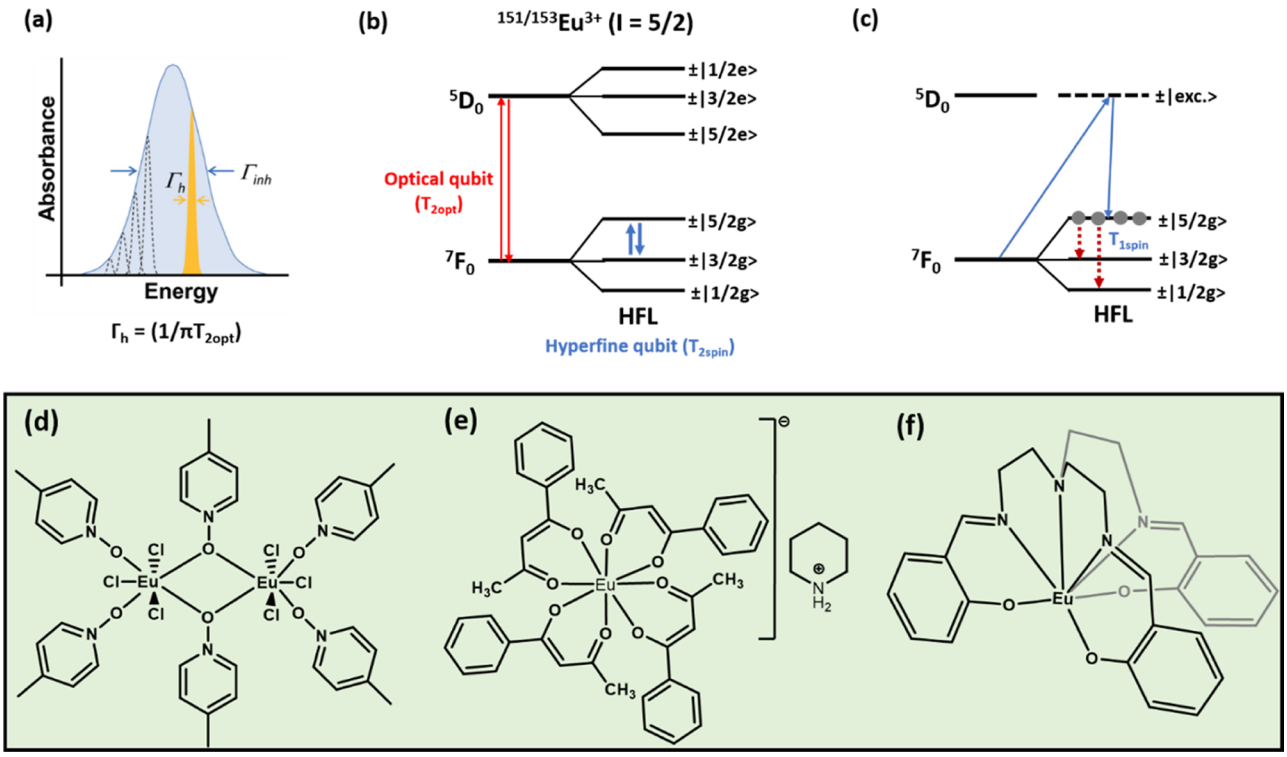

Figure 1. Concepts and molecular structures. (a) Schematic representation of an inhomogeneously broadened (Γ_{inh}) optical transition composed of homogeneously broadened (Γ_h) transitions. By selectively addressing a homogeneous line within the inhomogeneously broadened transition, spectral holes can be burnt. From the holewidth, the homogeneous linewidth can be estimated, which in turn can be used to estimate the optical coherence lifetime (T_{2opt}). (b) Electric dipole-induced $^5D_0 \rightarrow {}^7F_0$ transition associated with Eu^{3+} centers in a low symmetry ligand-field environment features narrow linewidths. The two stable isotopes of europium (^{151}Eu and ^{153}Eu) have nuclear spin (I) = 5/2; quadrupolar interaction between the electronic and nuclear spins leads to hyperfine splitting as shown in the figure. (c) Spectral-hole burning involves population redistribution in the ground-state HFLs, thereby nuclear spins are polarized; polarization in the ±|5/2g> level is assumed in the figure. Different spin lattice relaxation rates associated with the HFLs cause multiexponential hole decays. Molecular structures of the previously studied (d) seven coordinate binuclear ([Eu_2])[35] and (e) eight coordinate mononuclear ([Eu(BA)$]_4$(pip))[36] Eu^{3+} complexes. (f) Structure of the seven coordinate [Eu(trensal)] complex studied in this work. [Eu_2], [Eu(BA)$]_4$(pip), and [Eu(trensal)] complexes feature O_4Cl_3, O_8, and O_3N_4 coordination environments, respectively.

and manipulated optically, as reported for host lattices doped with Eu^{3+} centers.[9] The presence of an excited state ($^5D_0$) with sufficient lifetime (T_{1opt}) and ground-state hyperfine split levels (Figure 1b) renders Eu^{3+}-containing systems as lambda (Λ)-type quantum systems (Figure 1c). In such systems, the $^5D_0$ excited state can be used as an intermediate state to polarize the population in one of the hyperfine levels (HFLs)—for example, by applying two color photon pulses. Such state preparation enables the implementation of spin-wave storage quantum memory protocols for light, such as the atomic frequency comb (AFC) protocol. In the context of this study, nuclear spin polarization is observed from the spectral hole-burning (SHB) studies, as hole burning involves redistribution of nuclear spins in the ground-state HFLs, as schematically shown in Figure 1c, where population polarization in the ±|5/2g> level is assumed. In an ideal SHB experiment, a laser pulse of appropriate wavelength is applied to connect one of the ground HFLs to the $^5D_0$ level. Due to this optical pumping, the population is accumulated in the other two levels, as against the equally populated levels prior to laser excitation. Nuclear spin redistribution within the ground-state levels is multi-exponential in nature due to different mechanisms and consequent lifetimes, represented by T_{1spin} in Figure 1c, associated with the processes. The nuclear spin redistribution rates can be obtained by studying the spectral-hole depth as a function of time, as described in the Results and Discussion section.

Chemistry allows the tuning of linewidth and intensity (oscillator strength) of the $^5D_0 \rightarrow {}^7F_0$ transition by varying the ligand field geometry around the Eu^{3+} center. Additionally, isotopically enriched Eu^{3+}, complexes, either with ^{151}Eu or ^{153}Eu, can be synthesized following isotopological coordination chemistry, enabling the preparation of Eu^{3+} centers with control over hyperfine splitting energies. Consequently, we have recently demonstrated narrow $^5D_0 \rightarrow {}^7F_0$ optical transitions in bi-[35] (Figure 1d) and mono-nuclear (Figure 1e)[36] Eu^{3+} complexes. In the case of the binuclear complex, successful burning of spectral holes and consequent polarization of nuclear spins in the ground-state HFLs have been demonstrated. Remarkably, ultranarrow $^5D_0 \rightarrow {}^7F_0$ homogeneous linewidth translating as microsecond (μs) optical coherence lifetime has been observed for the mononuclear complex. Subsequently, we have demonstrated efficient polarization of nuclear spins in a particular HFL and storage of photons in the mononuclear complex. Crucially, the observation of optical coherence lifetime in the microsecond regime in stoichiometric (undiluted) mononuclear Eu^{3+}-complex crystals allowed us to demonstrate controlled Eu–Eu interactions, a step toward performing quantum gate operations.

Scheme 1. Preparation of [Eu(trensal)][a]

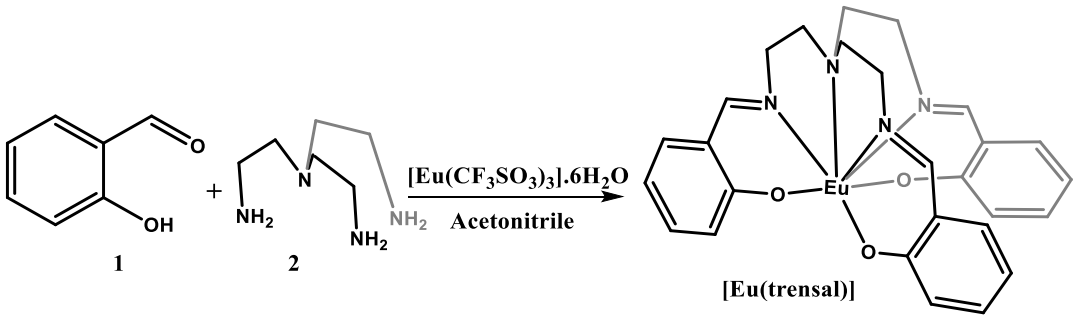

[a]Layering acetonitrile solution of salicylaldehyde (1) above acetonitrile solution containing tris(2-aminoethyl)amine (tren, 2) and [Eu(CF_3SO_3)·$6H_2O$] yielded the C_{3v} symmetric [Eu(trensal)] (CCDC: 2202838) as pencil-shaped crystals.

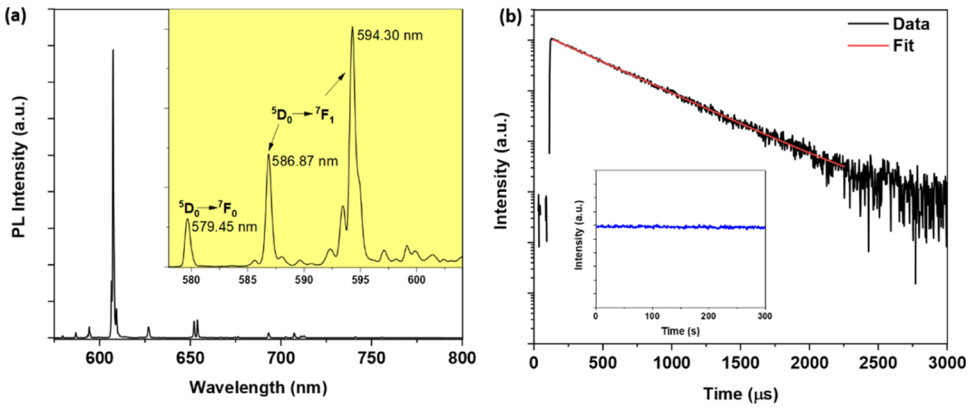

Figure 2. Emission characteristics of [Eu(trensal)] in the solid-state. (a) Steady-state emission spectrum of [Eu(trensal)] in the crystalline state. The inset shows the expanded spectrum in the 578−604 nm range; the $^5D_0 \rightarrow {}^7F_0$ and the $^5D_0 \rightarrow {}^7F_1$ transitions are labeled for clarity. The additional peaks around the $^5D_0 \rightarrow {}^7F_1$ transition are transitions from the excited ^5D_J (J = 1, 2, or 3) manifold to the ^7F_J manifold. (b) Time-resolved emission decay profile of [Eu(trensal)] in the solid-state monitored at 579 nm. A lifetime (T_{1opt}) of 354.05 μs was obtained by fitting the data with a mono-exponential function. The inset shows the photostability of the complex upon monitoring the emission intensity at 579 m for 300 s. All experiments were performed at about 2.3 K. An excitation wavelength of 380 nm was used, as inferred from the excitation spectrum shown in Figure S5.

The results discussed above indicate that europium complexes are particularly promising to feature narrow linewidths and long nuclear spin lifetimes (T_{1spin}). To check the validity of the statement, we have studied a prototypical charge-neutral mononuclear Eu^{3+} complex—[Eu(trensal)] (Figure 1f); trensal stands for 2,2′,2″-tris(salicylideneimino)-triethylamine. From the spectral-hole-burning studies at 4.2 K, we deduce a homogeneous linewidth of 2.8 MHz corresponding to an about 114 ns optical coherence lifetime (T_{2opt}). Nuclear spin lifetimes of 7 and 460 s, the longest so far reported for molecular systems, have been observed.

METHODS

Steady-state emission and excitation spectra were recorded using a Fluorolog-QM photoluminescence (PL) spectrometer (Figure S1) from HORIBA Scientific working with a continuous 75 W Xe lamp and a cooled Hamamatsu R928P photomultiplier in TE-cooled housing. The emission and excitation spectra were corrected for the instrumental artefacts using the manufacturer supplied correction factors. A 400 nm long pass filter was used to eliminate the second-order diffracted light. Phosphorescence lifetime measurements were performed using the same instrument and a pulsed Xe excitation light source. Errors on lifetimes are ±10%. The studies at about 2.3 K were performed by employing a cold-edge cold head (model number 101) connected with a SUMITOMO F-20 closed cycle He-cryostat. The complex was trapped in between two quartz plates and placed on the sample holder. Temperature was measured using a Lake Shore LS-335 temperature controller.

For the cryogenic ensemble spectroscopy experiments, a resonant excitation scheme and a home-built dipstick cryostat were used. The Sirah Matisse 2 DX dye laser has a full-width half maximum linewidth of about 100 kHZ and can be tuned over a large wavelength range; the wavelength for the experiments was adjusted at about 580 nm in order to match the coherent $^5D_0 \rightarrow {}^7F_0$ transition. The transmitted beam after the laser was guided through an acousto-optic modulator (AOM, Gooch-Housego: 3110-210) in the double pass configuration which is responsible for creating pulse sequences and frequency modulation. A second laser beam path was used as a reference path and was monitored via an optical spectrum analyzer to verify the laser frequency as well as to keep the laser running on a single mode. After the AOM, the light was fully fiber-coupled and guided to a small copper ferrule setup (Figure S2) containing the sample powder. The ferrule setup consisted of two opposing small cylindrical copper ferrules with a diameter of 1.25 mm; each ferrule had a bore size of 300 μm for the used multimode (MM) fiber with a core diameter of 200 μm.

One of the MM fibers was pulled back by 200 μm in the ferrule; this space served as a chamber for the sample powder. After the sample was put inside, both ferrules were fit in a Thorlabs ADAL4-5 mating sleeve connector and the whole ferrule setup was attached to a copper plate at the bottom of the dipstick cryostat. The temperature sensor was fixed next to the ferrule setup. The dipstick cryostat can be evacuated to a pressure of about 10^{-4} mbar. After evacuation, the dipstick was filled with He exchange gas and was dipped into liquid helium reaching down to 4.2 K experimental temperature. When exciting the sample via one fiber, the fluorescence light and the scattered light were collected via the second fiber and were finally guided either to a silicon photomultiplier module (SPM, KETEK, PE3315-WB-TIA-SP) or to a spectrometer (Andor-Shamrock-500i) to record PL spectra.

See sections S1–S4 for details concerning the preparation and characterization of [Eu(trensal)].

RESULTS AND DISCUSSION

Preparation and Low-Temperature Spectroscopic Studies of [Eu(trensal)]. [Eu(trensal)] is prepared following a previously reported literature procedure,[38] as depicted in Scheme 1; see section S3 for details. Single-crystal X-ray structure analysis of the pencil-shaped crystals of [Eu(trensal)] revealed that the complex crystallized in the $\bar{P}3c1$ space group belonging to the trigonal crystal system (Figure S4 and Table S1), as previously reported by Riley and co-workers.[39] Continuous shape measure analysis[40] revealed that the Eu^{3+} ion is placed in a C_{3v} symmetric ligand field, and the coordination geometry of [Eu(trensal)] is best described as a capped octahedron with a SHAPE index of 1.344 (Table S2).

For optical spectroscopy, we study the powder of the grown crystals compressed in a sample volume of about 4×10^{-2} mm^3. The complex shows characteristic Eu^{3+}-based emission upon excitation at 380 nm (Figure 2a) under cryogenic conditions at about 2.3 K. The $^5D_0 \rightarrow {}^7F_0$ transition was observed at 579.45 nm, as well as the other $^5D_0 \rightarrow {}^7F_J$ transitions. Compared to the previously studied mononuclear $[Eu(BA)]_4(pip)$ complex,[36] the $^5D_0 \rightarrow {}^7F_0$ transition is significantly stronger in comparison to the $^5D_0 \rightarrow {}^7F_1$ magnetic dipole transition which is independent of the ligand field. This indicates a higher branching ratio and thus a stronger light–matter coupling strength, which is an important aspect for further applications. Using pulsed excitation, an excited-state lifetime (T_{1opt}) of 354 μs was obtained (Figure 2b) upon monitoring the $^5D_0 \rightarrow {}^7F_0$ emission decay at 579 nm. The complex is photostable, as shown in the inset of Figure 2b. More details on the emission characteristics of the complex[41] are presented in section S6 (Figures S6–S8) of the Supporting Information.

The inhomogeneous linewidth of the coherent $^5D_0 \rightarrow {}^7F_0$ transition was measured by PL excitation spectroscopy at 4.2 K, using a dye laser tuned to about 580 nm. During the measurement, the laser was actively stabilized by using a reference cavity and its wavelength measured with a high-precision wavemeter. The fluorescence signal was separated from the excitation laser with a long-pass filter with a band edge at 594 nm. The dominant emission of the $^5D_0 \rightarrow {}^7F_2$ transition at about 607 nm and longer wavelengths was observed with a SPM. Multiple spectra were stitched together, and the resulting signal was fitted with a Lorentzian function, yielding a center wavelength of λ = 579.45 nm (Figure 3) and an inhomogeneous linewidth of 91 ± 0.4 GHz (full width at half maximum).

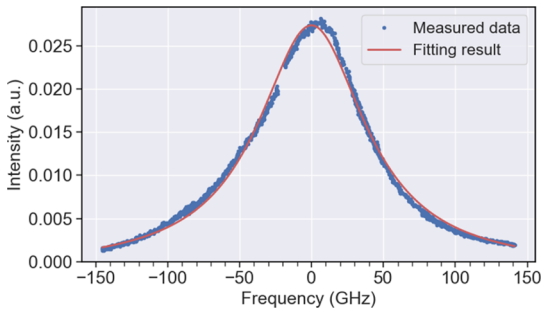

Figure 3. Inhomogeneous linewidth of [Eu(trensal)]. Excitation spectrum of the complex (blue dots). A Lorentzian fit (red line) gives a center wavelength of λ = 579.45 nm and an inhomogeneous linewidth of 91 ± 0.4 GHz.

Spectral Hole-Burning Studies. In order to measure the homogeneous linewidth, the SHB technique was applied. In SHB, a particular class of ions within the inhomogeneous line is addressed and optically pumped into other nuclear spin states. The depleted hyperfine state reveals a dip—that is, a spectral hole—in the fluorescence spectrum. The extracted spectral hole can be fitted with a Lorentzian function to obtain information on the homogeneous linewidth, as described in the Introduction section.

The pulse sequence used in all measurements consists of a 200 ms burning pulse and a 20 ms probe pulse followed by an erasing pulse sequence of 200 pulses with a duration of 20 ms each. In between different pulses, a delay time of 2 ms was set. Each SHB measurement is averaged 100 times and corrected for background. Before the final fitting, neighboring data points are binned together to smooth the data. The narrowest measured hole width for [Eu(trensal)] depicted in Figure 4a is 5.6 ± 0.2 MHz. Approximately 50% maximal hole contrast was observed for optimized parameters, demonstrating efficient optical pumping of HFLs. These measurements refer to the fluorescence signal measured by the SPM. In Figure 4b, the measurement was taken without a filter for the excitation light, with the intention of measuring an absorption signal in transmission.

For such a transmission measurement, the complex reveals a weak hole signal with a contrast of about 2% on top of a linear background. The best result for the spectral hole width is 5.6 ± 0.8 MHz and is consistent with the result of the SHB with the fluorescence signal. It was found that lower excitation power yielded the same spectral hole width as in the fluorescence measurements. We note that the contrast can be increased by optimizing the sample preparation which increases the optical depth.

One main broadening mechanism of the homogeneous linewidth is the incident laser power applied to drive the optical transition. By using the same pulse sequence as applied to the SHB but with varying power incident on the sample, we studied the laser power dependence of the homogeneous linewidth for [Eu(trensal)]. The dependence of the spectral hole contrast and holewidth on the laser power are depicted in Figure 5a,b, respectively. In this measurement, the maximum hole contrast was about 16%, which is more than a factor of 3 lower than in the previous measurement shown in Figure 4a. The two measurements were performed during two separate

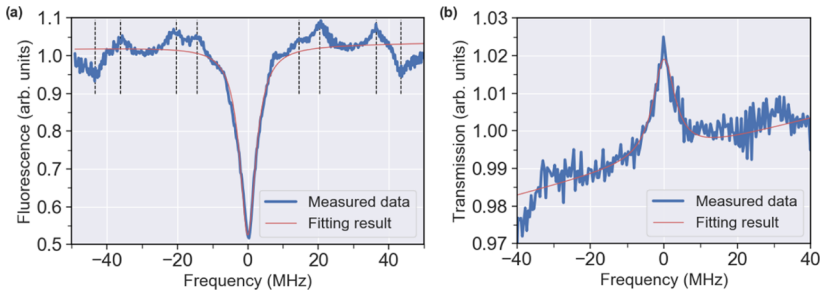

Figure 4. Homogeneous linewidth of [Eu(trensal)] obtained from SHB studies. (a) Fluorescence measurement in which the fluorescence is collected while scanning the dye laser (blue line). Besides the central hole, one can also see side holes at ±43.4 MHz and anti-holes at ±14.4, 20.4, and 36.3 MHz. A Lorentzian fit gives a central hole width of 5.6 ± 0.2 MHz (red line). (b) Absorption measurement where the total transmission is collected and normalized to a reference measurement. A hole width of 5.6 ± 0.8 MHz is obtained from a fit.

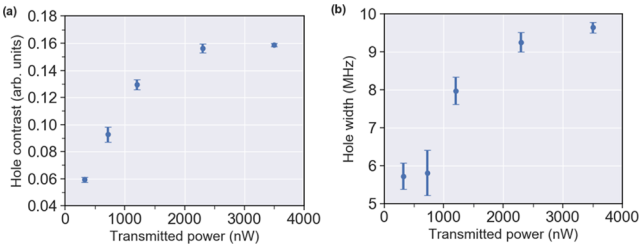

Figure 5. Laser power dependence of the homogeneous linewidth of [Eu(trensal)]. (a) Hole contrast and (b) hole widths were measured via SHB as a function of transmitted power.

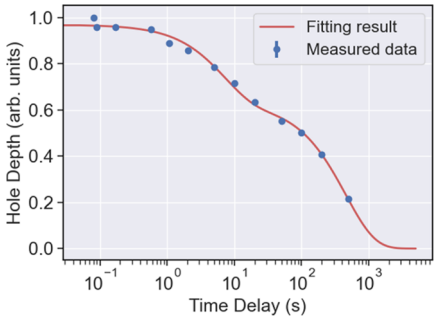

Figure 6. Nuclear spin lifetimes of [Eu(trensal)]. Data showing the evolution of hole depth as a function of time delay. A biexponential fit (red line) yields nuclear spin relaxation times of 7 ± 1 and 460 ± 80 s.

cooldowns, and we expect slight changes in the amount and configuration of the powder sample used in the preparation, leading to different optical depths. Due to high scattering losses within the powder, the resulting transmitted power was measured on the order of 1 μW. Both the homogeneous linewidth and the hole contrast were found to increase as a function of the pumping power. However, the measurements below 1000 nW transmitted power resulted in very low signal-to-noise ratios, limiting measurements at lower powers. This indicates that possibly even smaller hole widths can be observed when using different measurement techniques. For example, it is often found that photon echo measurements yield smaller homogeneous linewidths than the ones obtained from the SHB measurements. However, at this point, we were not able to observe photon echoes, probably due to insufficient optical depth of the prepared sample. This is consistent with the small hole contrast observed in the transmission measurement; see below for a discussion.

After hole burning, the hole depth will decay with time due to spin relaxation, as schematically shown in Figure 1c. To measure the nuclear spin lifetime (T_{1spin}), the same pulse sequence was used as described before but with a varying time delay between the burning and probe pulses. For each time delay, we measure at least 10 times and take the average hole depth value. Figure 6 shows the measured hole depth as a function of the time delay. The result is fitted with a double exponential function, yielding hole lifetimes of $\tau_1 = 7 \pm 1$ s and $\tau_2 = 460 \pm 80$ s, evidencing remarkably long nuclear spin lifetimes (T_{1spin}).

Two time constants associated with nuclear spin decay have been observed for the previously studied molecular complexes—[Eu_2] (unenriched) and [^{151}Eu(BA)$_4$][(pip)].[35,36] Non-monoexponential hole/nuclear spin-decay constants were also observed for Eu^{3+}:YSO (YSO stands for Y_2SiO_5), a non-molecular Eu^{3+} system.[42] The nuclear spin decay is caused by several mechanisms—for example, energy exchange with two level systems, direct one-phonon processes, two-step Orbach process, and inelastic Raman scattering, as discussed in the literature.[42] The different time constants associated with each mechanism for different HFLs (Figure 1c) could have caused biexponential hole decays in molecular systems. However, this tentative attribution needs to be ascertained by performing temperature and Eu^{3+}-concentration-dependent studies.

The above results elucidating narrow optical linewidths associated with the prototypical [Eu(trensal)] complex and similar results reported for [Eu_2] and [Eu(BA)$_4$][(pip)] complexes indicate that Eu^{3+} complexes can be pursued for creating coherent light−matter interfaces with QIP implications. In order to propose desirable molecular systems for QIP applications, in the following paragraphs, we attempt to establish a correlation between molecular structure and various parameters of QIP importance—T_{1opt}, f−f oscillator strength, Γ_{inh}, Γ_h, T_{2opt}, and T_{1spin} (Tables 1 and S4). To do so, we have considered the results obtained for the three molecular systems discussed in this study as well as the Γ_{inh}, Γ_h, and T_{2opt} values (Table S4) reported for stoichiometric $EuCl_3{\cdot}6H_2O$ and EuP_5O_{14} systems, as well as Eu^{3+}:YSO, an REI-impurity-doped solid-state system.

Excited-state lifetime (T_{1opt}) of a Eu^{3+} complex determines the lower limit of the homogeneous linewidth—that is, in the absence of external perturbations, the Γ_h is T_{1opt}-limited. This implies that having control over T_{1opt} is useful to obtain T_{1opt}-limited Γ_h. Multi-phonon relaxation pathways facilitate non-radiative deactivation of excited states in Eu^{3+} complexes (Figure S9).[43] The C−H, O−H, and N−H vibrations (νX−H (cm^{-1}); X = C, O, or N) featuring a high anharmonicity parameter in the vicinity of the Eu^{3+} centers cause non-

Table 1. Experimentally Determined Excited-State Lifetimes (T_{1opt}), Inhomogeneous (Γ_{inh})- and Homogeneous (Γ_h)-Linewidths, Optical Coherence Lifetimes (T_{2opt}), and Nuclear Spin Lifetimes (T_{1spin}) Associated with the Complexes Discussed in This Study

molecule	T_{1opt}	Γ_{inh}	Γ_h	T_{2opt}	T_{1spin}
$[Eu_2]$	880 μs (20 K)	50 GHz (1.4 K)	22 ± 1 MHz (1.4 K)	14.5 ns (1.4 K)[a]	1.6 ± 1 and >30 s (1.4 K)
$[Eu(BA)]_4$(pip)	540 μs (1.4 K)	6.6 ± 0.1 GHz (1.4 K)	30.2 ± 0.6 kHz (1.4 K)	10.5 μs (1.4 K)[b]	430 ± 100 ms and 300 ± 30 s (1.4 K)
[Eu(trensal)]	354.05 μs (2.3 K)	91 ± 0.4 GHz (4.2 K)	2.8 MHz (4.2 K)	114 ns (4.2 K)[a]	7 ± 1 s and 460 ± 80 s (4.2 K)

[a]From SHB studies. [b]From photon echo measurements.

radiative deactivation of the $^5D_0$ excited state, thereby excited-state lifetimes (T_{1opt}) are reduced.[44] The ligand field symmetry around the emissive Eu^{3+} center is another parameter having a role on the excited-state lifetime.[45−47] It is reported that a low ligand field symmetry around Eu^{3+} increases the radiative decay constant (k_r), reducing T_{1opt}. Consequently, relatively small T_{1opt} values are expected for Eu^{3+} centers placed in an asymmetric ligand field environment than the ones placed in a symmetric environment. Based on the above conceptual framework, conclusions relating to molecular structures and T_{1opt} are presented for the three Eu^{3+} complexes discussed in this study, as follows.

T_{1opt} values of the complexes discussed in this study are arranged in the following order: $[Eu_2]$ > $[Eu(BA)_4][(pip)]$ > [Eu(trensal)] (Table 1). In the cases of $[Eu(BA)_4][(pip)]$ and [Eu(trensal)], there are C−H oscillators in the close vicinity of the Eu^{3+} center; see structures in Figure 1d−f. On the other hand, the C−H oscillators are relatively far away from Eu^{3+} in $[Eu_2]$. Consequently, one can infer the dominant role of the multi-phonon non-radiative deactivation mechanism in reducing the $^5D_0$ excited-state lifetime in [Eu(trensal)]. To ascertain the role of symmetry and anharmonic vibrations causing lifetime reduction, we have estimated the radiative (K_r) and non-radiative (K_{nr}) decay constants (Table S5) of the complexes; see previous work for details.[35] The K_r value obtained for [Eu(trensal)] is greater than the ones obtained for the remaining complexes. This indicates a faster deactivation of the excited state in [Eu(trensal)] compared to that in $[Eu_2]$ and $[Eu(BA)_4][(pip)]$, explaining the trend in the T_{1opt}. The large magnitude of K_{nr} calculated for [Eu(trensal)] elucidates competing non-radiative pathways contributing to the deactivation of the excited state in the complex, as discussed above. The above facets imply that ligand field symmetry and anharmonic oscillators around Eu^{3+} go hand-in-hand in reducing the T_{1opt} of [Eu(trensal)].

From the QIP perspective, T_{1opt} is a limiting factor determining the upper bound of T_{2opt}. That is, large T_{1opt} values result as a narrow homogeneous linewidth with a consequent increase in T_{2opt}, as compiled in Table S4. Therefore, molecular complexes with large T_{1opt} are desirable to have small T_{1opt}-limited homogeneous linewidths. The advantage of molecular systems is the possibility of T_{1opt} tuning adopting to molecular design strategies, as exemplified in the case of $EuCl_3{\cdot}6H_2O$. By preparing the deuterated version of the complex—$EuCl_3{\cdot}6D_2O$—about 1 order of increase in T_{1opt} was achieved with a consequent T_{2opt} increase (see Table S4).[48]

The oscillator strength of the electric-dipole-induced $^5D_0 \rightarrow {}^7F_0$ transition is one of the defining factors determining the strength of the light−matter interactions. One of the main mechanisms causing the occurrence of the transition is *J*-mixing—that is, the $^7F_0$ ground-state wavefunction is best described as a mixture of the $^7F_0$ ground state and other excited states—$^7F_2$ ($M_J = 0$), for example.[45] Deviation from a centrosymmetric point group to a non-centrosymmetric point group is shown to facilitate the *J*-mixing, thereby the $^5D_0 \rightarrow {}^7F_0$ oscillator strength in Eu^{3+} complexes gains intensity.[45] The above facet elucidates that it is possible to establish a correlation between the ligand field symmetry and oscillator strength of the $^5D_0 \rightarrow {}^7F_0$ transition. Among the three complexes discussed in this article, the $^5D_0 \rightarrow {}^7F_0$ oscillator strength of [Eu(trensal)] is higher than the ones obtained for $[Eu_2]$ and $[Eu(BA)_4]$(pip) (Figure S10). The comparison indicates that the Eu^{3+} center in [Eu(trensal)] is placed in a low symmetric environment relative to ones in the $[Eu(BA)_4]$-(pip) and $[Eu_2]$. The above statement is consistent with the site symmetry of the complexes obtained from single-crystal X-ray diffraction studies (Figure S11). A point noteworthy here is that the $^5D_0 \rightarrow {}^7F_0$ transition is not allowed for the D_{5h} and D_{4d} crystallographic symmetries obtained for $[Eu_2]$ and $[Eu(BA)_4]$(pip), respectively, from the SHAPE analysis (Figure S11). Deformation of the coordination geometries of the complexes to relatively low-symmetric ones could have allowed the $^5D_0 \rightarrow {}^7F_0$ transition to gain intensity. The assumption is in line with the observations reported for $EuCl_3{\cdot}6H_2O$—D_{4d} and C_2 geometries were inferred from the crystallographic and spectroscopic studies, respectively.[49]

An optical transition is inhomogeneously broadened (Γ_{inh}) mainly due to the defects and imperfections present in a crystal lattice. The broadening is an important parameter determining the storage density of optical quantum memories (vide infra). In the case of Eu^{3+}:YSO, Γ_{inh} as a function of doping concentration was studied and a linear increase in Γ_{inh} with concentration was observed.[42] The increase in linewidth with increasing Eu^{3+} doping level (concentration) was attributed to the strain caused by the Eu^{3+} dopant (impurity) in the YSO host lattice due to the ionic radii difference (mismatch) between the Eu^{3+} (108.7 pm) and Y^{3+} (104 pm) ions. At 7% Eu^{3+} concentration, Γ_{inh} = 150 GHz was reported for Eu^{3+}:YSO at 2 K. The value is larger than the ones (Table 1) estimated for [Eu(trensal)], $[Eu_2]$, and $[Eu(BA)_4]$pip complexes. Considering the stoichiometric content of the Eu^{3+} molecular crystals, the strain-induced broadening due to ionic radius mismatch is ruled out for the molecular crystals. Apart from the three complexes discussed in this study, Γ_{inh} values were estimated for two other stoichiometric crystals—$EuCl_3{\cdot}6H_2O$ and EuP_5O_{14}. The reported Γ_{inh} = 0.1 GHz and 3.5 GHz for $EuCl_3{\cdot}6H_2O$[48] and EuP_5O_{14},[50] respectively, indicate the high crystalline quality of the samples.

Based on the above discussion, we attribute the smaller Γ_{inh} in the stoichiometric molecular crystals, relative the one observed for 7% Eu^{3+}:YSO, to the absence of dopant-induced defects in the crystal lattice. The Γ_{inh} within the molecular series increases in the following order: $[Eu(BA)_4][(pip)]$ < $[Eu_2]$ < [Eu(trensal)]. The tens of GHz range Γ_{inh} associated with $[Eu_2]$ and [Eu(trensal)] is tentatively attributed to the

inferior crystalline quality associated with the complexes relative to $[Eu(BA)_4][(pip)]$.

The inhomogeneous line broadening observed in REI-impurity-doped host lattices and molecular complexes are useful to obtain optical quantum memories based on the AFC protocol. The possible selection of frequency modes within an inhomogeneously broadened optical transition allows for frequency multiplexed photon storage. In this context, the Γ_{inh}/Γ_h ratio determines the maximum possible number of modes that can be addressed within Γ_{inh}, determining the bandwidth.[42] Although the Γ_{inh}/Γ_h ratio is frequently discussed in the literature, Ortu et al.,[51] recently proposed another methodology to calculate the number of available modes. The authors described that the number of available frequency modes (N_f) within an inhomogeneously broadened optical transition depends on the sum of the frequency spacing between the ground (Δg) and excited (Δe) HFLs and the width of the absorption teeth (Δf); see eq 1.

$$N_f = \Gamma_{inh}/2(\Delta g + \Delta e) + \Delta f \quad (1)$$

Using eq 1, N_f values of 179, 24, and 325 have been calculated for $[Eu_2]$, $[Eu(BA)_4](pip)$, and [Eu(trensal)], respectively. Note, in the calculations we have used $\Delta g + \Delta e$ = 139.6 MHz and Δf = 0.9 MHz obtained for $[^{151}Eu(BA)_4]$-(pip). This is the best possible approximation in the absence of hyperfine splitting energetics for $[Eu_2]$ and [Eu(trensal)] and AFC experiments. In any case, the N_f values calculated for the complexes follow the trend observed from the Γ_{inh}/Γ_h ratios (Table S6). Importantly, the calculated N_f values or Γ_{inh}/Γ_h ratios indicate that a wide Γ_{inh} is beneficial for optical quantum memory applications. If one considers the available bandwidth of the memory, large hyperfine splitting between the levels is desirable. Therefore, ^{153}Eu-enriched complexes are suitable for the quantum memory applications, though with a compromise on N_f.

The homogeneous linewidth (Γ_h) associated with an optical transition determines the optical coherence lifetime (T_{2opt}). In an ideal scenario, the homogeneous linewidth is determined by the excited-state lifetime (T_{1opt}), the lifetime of the $^5D_0$ excited state in the context of this study. As discussed above, T_{1opt}-limited Γ_h can be controlled by varying the symmetry around the Eu^{3+} center and reducing the contributions from non-radiative deactivation mechanisms by varying isotopic composition of ligands. Consequently, a molecular control over the lower limit of Γ_h and the upper limit of QIP-relevant parameter T_{2opt} can be achieved. However, T_{1opt}-limited Γ_h are often not observed (see Table S4). The additional line-broadening is caused by mechanisms such as interaction between the REIs with lattice phonon modes, inter REI−REI interaction (dipolar interaction), and interaction between the REIs and the nuclear spins in a host lattice.

In the following, we refer to some case studies and attempt to highlight various factors that can potentially contribute to line broadening in molecular systems. The effect of J-mixing on T_{2opt} was elucidated by Tanaka and Kushida for Eu^{3+}:YSO.[52] The mixing of the $^7F_0$ ground-state wavefunction with the $^7F_2$ state contributes to the reduction in T_{2opt} value because J-mixing facilitates the coupling of the $^5D_0 \rightarrow {}^7F_0$ transition dipole with two level systems (nuclear spin flips, for example) and one phonon-mediated $^7F_0$−$^7F_1$ absorption processes. From the above it can be inferred that the J-mixing mechanism causing the increase in the $^5D_0 \rightarrow {}^7F_0$ transition probability can also contribute to T_{2opt} reduction.

Narrow homogeneous linewidths associated with the $^5D_0 \rightarrow {}^7F_0$ transition are reported for the stoichiometric $EuCl_3\cdot 6H_2O$[48] and EuP_5O_{14}[50] systems. Homogeneous linewidths of 4.1 kHz (below 4 K, as reported in the original study) and 32 kHz (2 K) were estimated for $EuCl_3\cdot 6H_2O$ and EuP_5O_{14}, respectively, from the photon echo measurements. For $EuCl_3\cdot 6H_2O$, the experimental Γ_h (4.1 kHz) is close to the T_{1opt}-limited one (1.37 kHz). On the other hand, for EuP_5O_{14} the experimentally obtained Γ_h (32 kHz) is 3 orders greater than the T_{1opt}-limited one (31.82 Hz). The significant differences between the lifetime-limited and experimental Γ_h values reported for EuP_5O_{14} indicate the operation of strong dephasing mechanisms contributing to the line broadening; one possible mechanism could be the spin fluctuations stemming from the nuclear spin bath associated with ^{31}P atoms. In the case of $EuCl_3\cdot 6H_2O$, significant improvements on T_{1opt}, Γ_h, and T_{2opt} (see Table S4 for comparisons) were achieved after deuterium enrichment ($EuCl_3\cdot 6D_2O$), implying the role of molecular vibrations contributing to the decoherence of the superposition states.

As far as the molecular systems discussed in this study are concerned, we make a comparison between the Γ_h and T_{2opt} values obtained from the SHB studies because linewidths measured from photon echo measurements are always narrower than the ones obtained from the SHB studies. The fact is exemplified in the case of $[Eu(BA)_4][(pip)]$; Γ_h = 0.15 MHz (T_{2opt} = 0.91 μs) and 0.37 MHz (T_{2opt} = 0.37 μs) were estimated from photon echo and SHB studies, respectively, at 4 K.[36] Quantitatively, for $[Eu(BA)_4][(pip)]$, the linewidth estimated from SHB is 2.5 times broader than the one from photon echo. The Γ_h = 2.8 MHz estimated for [Eu(trensal)] at 4.2 K from the SHB study is an order of magnitude broader than the linewidth obtained for $[Eu(BA)_4][(pip)]$ at 4 K. The comparison indicates that the Γ_h depends on the temperature. In the case of the binuclear complex—$[Eu_2]$—Γ_h = 22 MHz was estimated from the SHB studies at 1.4 K, and no photon echo data is available. To compare the Γ_h values of the binuclear and mononuclear $[Eu(BA)_4][(pip)]$ (Γ_h = 30.3 kHz) complexes obtained from the SHB and photon echo studies, respectively, at 1.4 K, we assumed a PE equivalent linewidth of about 8.8 MHz for the binuclear complex by using the factor of 2.5 observed for the mononuclear complex. It is clear from the above comparison that significantly broader linewidth was observed for the binuclear complex relative to $[Eu(BA)_4]$-$[(pip)]$. We attribute the difference to the presence of strong intra Eu^{3+}−Eu^{3+} dipolar interactions in $[Eu_2]$ mediated by close intra Eu^{3+}−Eu^{3+} distances (Figure S12).

In many QIP schemes, information is stored in the hyperfine states and readout on demand.[9] Therefore, long nuclear spin lifetimes (T_{1spin}) are desirable. A specific example concerns quantum memories where long T_{1spin} are desirable because this might lead to long T_{2spin} (hyperfine coherence time). In the case of a multimodal quantum network, T_{2spin} in the order of seconds are desirable, requiring long T_{1spin} for the optical manipulation of spins at will. The remarkable observations of long optical coherence (T_{2opt}), which is a lower bound for T_{2spin}, and T_{1spin} life times in stoichiometric molecular crystals indicate that REI-based molecular crystals could serve not only as good qubit candidates but also as efficient optical memories. Although we invoke the term "stoichiometric" to show that all sites are occupied by optically active Eu^{3+} centers, one should consider the presence of organic ligands around the emissive

Eu^{3+} centers, reducing the effective concentration of optically active ions in the crystal lattice.

All optical coherent control over nuclear spins has been demonstrated for Eu^{3+}-doped nanoparticles[53] and Eu^{3+}:YSO.[9] As in the case of T_{2opt}, the presence of nuclear spin fluctuations in the surroundings reduces the T_{2spin}. By applying an external magnetic field, the nuclear spin fluctuations can be frozen, thereby T_{2opt} and T_{2spin} can be increased. As far as molecular systems are concerned, the role of external magnetic field on coherence lifetimes is yet to be demonstrated—a possibility that can be leveraged to increase the QIP utility of molecular complexes.

Based on the above discussion, we propose the following molecular-design considerations to realize efficient light–matter interactions in Eu^{3+} complexes. It is imperative to have the Eu^{3+} center in a low symmetric ligand-field environment, facilitating the $^5D_0 \rightarrow {}^7F_0$ transition to gain oscillator strength. A minimal presence of nuclear spins in coordinating ligands and the presence of rigid ligand frameworks are desirable to mitigate the spin-bath and lattice vibrations, respectively, contributing to decoherence. To implement SHB and photon echo sequences, Eu^{3+} complexes featuring excited-state lifetimes (T_{1opt}) in the order of hundreds of microseconds are desirable. Complexes with large T_{1opt} are also desirable to obtain small lifetime-limited Γ_h. This can be achieved by tuning the ligand structure, as done in the case of $EuCl_3{\cdot}6H_2O$ where deuteration ($EuCl_3{\cdot}6D_2O$) is shown to improve the T_{1opt}. Apart from the above, Eu^{3+} complexes need to be prepared and crystallized in a reproducible manner, and they should be stable under ambient conditions, engendering them with practical utility. The presence of lattice solvent is a concern. A loss of lattice solvent is possible in some cases, reducing the quality of the crystal by creating defects, which will increase line broadening. Therefore, preparation of lattice-solvent-free Eu^{3+} complexes is desirable. However, the endeavor is not entirely at the disposal of a chemist; a systematic screening is the only possibility to obtain lattice-solvent-free crystals. Although weak, dipolar interactions between optically active Eu^{3+} centers contribute to the decoherence of superposition states. The interaction can be mitigated by diluting a Eu^{3+} complex in an isostructural non-emissive host lattice.[36] In order to effect the dilution, an isostructural Y^{3+} ($I = 1/2$) complex needs to be prepared.

The possibility of obtaining well-defined molecular crystals with tuneable optical properties and doping concentration and isotopic enrichment are encouraging to pursue Eu^{3+} complexes as coherent light–matter interfaces. However, so far, only three Eu^{3+} complexes (Figure 1d–f) have been studied as coherent light–matter interfaces. Further studies covering a range of structurally different Eu^{3+} complexes are necessary to elucidate various mechanisms governing QIP-related parameters and to probe if the narrow linewidths are a ubiquitous property of all Eu^{3+} complexes showing the $^5D_0 \rightarrow {}^7F_0$ transition.

It would be also interesting to study Yb^{3+} and Er^{3+} complexes that emit in the near-infra-red region because such complexes are useful for realizing molecule-based quantum communication architectures.[18,54] Two recent reports elucidate narrow optical linewidths associated with Yb^{3+} complexes,[55,56] implying the utility of Ln^{3+} complexes for creating coherent light–matter interfaces with quantum technological implications.

CONCLUSIONS

The present study demonstrates narrow optical linewidths and long nuclear spin lifetimes associated with the prototypical [Eu(trensal)] complex. Similar results obtained for two other Eu^{3+} complexes, [Eu_2] and [$Eu(BA)_4$][(pip)], featuring different coordination environments indicate that Eu^{3+} complexes showing the $^5D_0 \rightarrow {}^7F_0$ optical transition could be considered as tuneable molecular platforms for implementing QIP schemes. The presence of an excited state connected to the ground-state hyperfine split levels renders molecular Eu^{3+} complexes as lambda (Λ)-type quantum systems. By taking advantage of this, we have demonstrated efficient optical pumping of HF levels of [Eu(trensal)], a central starting point for coherent optical spin rotation and the consequent full qubit control. Such state preparation (spin polarization) enables, for example, the implementation of spin-wave storage quantum memory protocols for light, such as the AFC protocol in molecular systems, as demonstrated for [$Eu(BA)_4$][(pip)]. Additionally, by taking advantage of long T_{1spin} and coherently driving nuclear spin transitions using radio frequencies,[9] molecule-based nuclear spin qubits with long spin coherence times (T_{2spin}) can be prepared and manipulated, a challenging proposal that needs be realized for molecular systems.

Overall, the results presented in this study for [Eu(trensal)], comparisons made with the previously reported stoichiometric Eu^{3+}-based systems, and the consequent proposals on molecular design requirements to enable control over the QIP-relevant parameters—T_{1opt}, Γ_{inh}, and Γ_h—can be leveraged to obtain Eu^{3+} complexes as coherent light–matter interfaces for QIP applications.

AUTHOR INFORMATION

Corresponding Authors

Senthil Kumar Kuppusamy – *Institute of Quantum Materials and Technologies (IQMT), Karlsruhe Institute of Technology (KIT), Eggenstein-Leopoldshafen 76344, Germany;* orcid.org/0000-0002-1501-7759; Email: senthil.kuppusamy2@kit.edu

David Hunger – *Institute of Quantum Materials and Technologies (IQMT), Karlsruhe Institute of Technology (KIT), Eggenstein-Leopoldshafen 76344, Germany; Physikalisches Institut (PHI), Karlsruher Institut für*

Technologie (KIT), Karlsruhe 76131, Germany; orcid.org/0000-0001-6156-6145; Email: david.hunger@kit.edu

Mario Ruben − *Institute of Quantum Materials and Technologies (IQMT), Karlsruhe Institute of Technology (KIT), Eggenstein-Leopoldshafen 76344, Germany; Institute of Nanotechnology (INT), Karlsruhe Institute of Technology (KIT), Eggenstein-Leopoldshafen 76344, Germany; Centre Européen de Sciences Quantiques (CESQ), Institut de Science et d'Ingénierie Supramoléculaires (ISIS), Strasbourg Cedex 67083, France*; Email: mario.ruben@kit.edu

Authors

Evgenij Vasilenko − *Institute of Quantum Materials and Technologies (IQMT), Karlsruhe Institute of Technology (KIT), Eggenstein-Leopoldshafen 76344, Germany; Physikalisches Institut (PHI), Karlsruher Institut für Technologie (KIT), Karlsruhe 76131, Germany*

Weizhe Li − *Physikalisches Institut (PHI), Karlsruher Institut für Technologie (KIT), Karlsruhe 76131, Germany;* orcid.org/0000-0002-6277-0399

Jannis Hessenauer − *Physikalisches Institut (PHI), Karlsruher Institut für Technologie (KIT), Karlsruhe 76131, Germany*

Christina Ioannou − *Physikalisches Institut (PHI), Karlsruher Institut für Technologie (KIT), Karlsruhe 76131, Germany;* Present Address: QuTech TU Delft, Lorentzweg 1, 2628 CJ Delft, The Netherlands

Olaf Fuhr − *Institute of Nanotechnology (INT) and Karlsruhe Nano Micro Facility (KNMFi), Karlsruhe Institute of Technology (KIT), Eggenstein-Leopoldshafen 76344, Germany*

Notes

The authors declare no competing financial interest.

ACKNOWLEDGMENTS

This study is dedicated to Prof. Dieter Fenske for his unwavering support related to single-crystal X-ray diffraction studies. We thank the anonymous reviewers for their constructive criticism and remarks, which helped us to improve the quality of the manuscript. We thank Dr. Philippe Goldner and Dr. Diana Serrano, Chimie ParisTech, PSL University, CNRS, Institut de Recherche de Chimie Paris, Paris, France, for helpful discussions. We thank Dr. Sergei Lebedkin, KIT, for his support and guidance during the installation of the PL spectrometer. Karlsruhe Nano Micro Facility (KNMFi), Karlsruhe Institute of Technology (KIT), is thanked for the facilities. S.K.K. and M.R. thank KIT-future fields stage 1 programme for funding the project "organising molecular qubits through molecular self-assembly". D.H. and M.R. thank KIT-future fields stage 3 programme for funding the project "optically addressable molecular qubits for quantum networks". D.H. and M.R. thank Deutsche Forschungsgemeinschaft (DFG, German Research Foundation) for funding collaborative research centre 1573 (CRC1573) "4f for future" under the cluster of excellence scheme.

REFERENCES

(1) DiVincenzo, D. P. The Physical Implementation of Quantum Computation. *Fortschr. Phys.* **2000**, *48*, 771−783.

(2) Heinrich, A. J.; Oliver, W. D.; Vandersypen, L. M. K.; Ardavan, A.; Sessoli, R.; Loss, D.; Jayich, A. B.; Fernandez-Rossier, J.; Laucht, A.; Morello, A. Quantum-Coherent Nanoscience. *Nat. Nanotechnol.* **2021**, *16*, 1318−1329.

(3) Gruber, A.; Dräbenstedt, A.; Tietz, C.; Fleury, L.; Wrachtrup, J.; Borczyskowski, C. von. Scanning Confocal Optical Microscopy and Magnetic Resonance on Single Defect Centers. *Science* **1997**, *276*, 2012−2014.

(4) Jelezko, F.; Gaebel, T.; Popa, I.; Gruber, A.; Wrachtrup, J. Observation of Coherent Oscillations in a Single Electron Spin. *Phys. Rev. Lett.* **2004**, *92*, 076401.

(5) Bar-Gill, N.; Pham, L. M.; Jarmola, A.; Budker, D.; Walsworth, R. L. Solid-State Electronic Spin Coherence Time Approaching One Second. *Nat. Commun.* **2013**, *4*, 1743.

(6) Babin, C.; Stöhr, R.; Morioka, N.; Linkewitz, T.; Steidl, T.; Wörnle, R.; Liu, D.; Hesselmeier, E.; Vorobyov, V.; Denisenko, A.; et al. Fabrication and Nanophotonic Waveguide Integration of Silicon Carbide Colour Centres with Preserved Spin-Optical Coherence. *Nat. Mater.* **2022**, *21*, 67−73.

(7) Lukin, D. M.; Guidry, M. A.; Vučković, J. Integrated Quantum Photonics with Silicon Carbide: Challenges and Prospects. *PRX Quantum* **2020**, *1*, 020102.

(8) Higginbottom, D. B.; Kurkjian, A. T. K.; Chartrand, C.; Kazemi, M.; Brunelle, N. A.; MacQuarrie, E. R.; Klein, J. R.; Lee-Hone, N. R.; Stacho, J.; Ruether, M.; et al. Optical Observation of Single Spins in Silicon. *Nature* **2022**, *607*, 266−270.

(9) Zhong, M.; Hedges, M. P.; Ahlefeldt, R. L.; Bartholomew, J. G.; Beavan, S. E.; Wittig, S. M.; Longdell, J. J.; Sellars, M. J. Optically Addressable Nuclear Spins in a Solid with a Six-Hour Coherence Time. *Nature* **2015**, *517*, 177−180.

(10) Thiele, S.; Balestro, F.; Ballou, R.; Klyatskaya, S.; Ruben, M.; Wernsdorfer, W. Electrically Driven Nuclear Spin Resonance in Single-Molecule Magnets. *Science* **2014**, *344*, 1135−1138.

(11) Shiddiq, M.; Komijani, D.; Duan, Y.; Gaita-Ariño, A.; Coronado, E.; Hill, S. Enhancing Coherence in Molecular Spin Qubits via Atomic Clock Transitions. *Nature* **2016**, *531*, 348−351.

(12) Bayliss, S. L.; Laorenza, D. W.; Mintun, P. J.; Kovos, B. D.; Freedman, D. E.; Awschalom, D. D. Optically Addressable Molecular Spins for Quantum Information Processing. *Science* **2020**, *370*, 1309−1312.

(13) Moreno-Pineda, E.; Godfrin, C.; Balestro, F.; Wernsdorfer, W.; Ruben, M. Molecular Spin Qudits for Quantum Algorithms. *Chem. Soc. Rev.* **2018**, *47*, 501−513.

(14) Gaita-Ariño, A.; Luis, F.; Hill, S.; Coronado, E. Molecular Spins for Quantum Computation. *Nat. Chem.* **2019**, *11*, 301−309.

(15) Wasielewski, M. R.; Forbes, M. D. E.; Frank, N. L.; Kowalski, K.; Scholes, G. D.; Yuen-Zhou, J.; Baldo, M. A.; Freedman, D. E.; Goldsmith, R. H.; Goodson, T.; et al. Exploiting Chemistry and Molecular Systems for Quantum Information Science. *Nat. Rev. Chem.* **2020**, *4*, 490−504.

(16) Atzori, M.; Sessoli, R. The Second Quantum Revolution: Role and Challenges of Molecular Chemistry. *J. Am. Chem. Soc.* **2019**, *141*, 11339−11352.

(17) Ardavan, A.; Rival, O.; Morton, J. J. L.; Blundell, S. J.; Tyryshkin, A. M.; Timco, G. A.; Winpenny, R. E. P. Will Spin-Relaxation Times in Molecular Magnets Permit Quantum Information Processing? *Phys. Rev. Lett.* **2007**, *98*, 057201.

(18) Laorenza, D. W.; Freedman, D. E. Could the Quantum Internet Be Comprised of Molecular Spins with Tunable Optical Interfaces? *J. Am. Chem. Soc.* **2022**, *144*, 21810−21825.

(19) Nakazawa, S.; Nishida, S.; Ise, T.; Yoshino, T.; Mori, N.; Rahimi, R. D.; Sato, K.; Morita, Y.; Toyota, K.; Shiomi, D.; et al. A Synthetic Two-Spin Quantum Bit: G -Engineered Exchange-Coupled Biradical Designed for Controlled-NOT Gate Operations. *Angew. Chem., Int. Ed.* **2012**, *51*, 9860−9864.

(20) Morton, J. J. L.; Tyryshkin, A. M.; Ardavan, A.; Porfyrakis, K.; Lyon, S. A.; Andrew D Briggs, G. Electron Spin Relaxation of N@C60 in CS2. *J. Chem. Phys.* **2006**, *124*, 014508.

(21) Zadrozny, J. M.; Gallagher, A. T.; Harris, T. D.; Freedman, D. E. A Porous Array of Clock Qubits. *J. Am. Chem. Soc.* **2017**, *139*, 7089−7094.
(22) Zadrozny, J. M.; Niklas, J.; Poluektov, O. G.; Freedman, D. E. Multiple Quantum Coherences from Hyperfine Transitions in a Vanadium(IV) Complex. *J. Am. Chem. Soc.* **2014**, *136*, 15841−15844.
(23) Tesi, L.; Lucaccini, E.; Cimatti, I.; Perfetti, M.; Mannini, M.; Atzori, M.; Morra, E.; Chiesa, M.; Caneschi, A.; Sorace, L.; et al. Quantum Coherence in a Processable Vanadyl Complex: New Tools for the Search of Molecular Spin Qubits. *Chem. Sci.* **2016**, *7*, 2074−2083.
(24) Atzori, M.; Morra, E.; Tesi, L.; Albino, A.; Chiesa, M.; Sorace, L.; Sessoli, R. Quantum Coherence Times Enhancement in Vanadium(IV)-Based Potential Molecular Qubits: The Key Role of the Vanadyl Moiety. *J. Am. Chem. Soc.* **2016**, *138*, 11234−11244.
(25) Atzori, M.; Tesi, L.; Morra, E.; Chiesa, M.; Sorace, L.; Sessoli, R. Room-Temperature Quantum Coherence and Rabi Oscillations in Vanadyl Phthalocyanine: Toward Multifunctional Molecular Spin Qubits. *J. Am. Chem. Soc.* **2016**, *138*, 2154−2157.
(26) Yu, C.-J.; Graham, M. J.; Zadrozny, J. M.; Niklas, J.; Krzyaniak, M. D.; Wasielewski, M. R.; Poluektov, O. G.; Freedman, D. E. Long Coherence Times in Nuclear Spin-Free Vanadyl Qubits. *J. Am. Chem. Soc.* **2016**, *138*, 14678−14685.
(27) Bader, K.; Dengler, D.; Lenz, S.; Endeward, B.; Jiang, S.-D.; Neugebauer, P.; van Slageren, J. Room Temperature Quantum Coherence in a Potential Molecular Qubit. *Nat. Commun.* **2014**, *5*, 5304.
(28) Bader, K.; Winkler, M.; van Slageren, J. Tuning of Molecular Qubits: Very Long Coherence and Spin−Lattice Relaxation Times. *Chem. Commun.* **2016**, *52*, 3623−3626.
(29) Yamabayashi, T.; Atzori, M.; Tesi, L.; Cosquer, G.; Santanni, F.; Boulon, M.-E.; Morra, E.; Benci, S.; Torre, R.; Chiesa, M.; et al. Scaling Up Electronic Spin Qubits into a Three-Dimensional Metal−Organic Framework. *J. Am. Chem. Soc.* **2018**, *140*, 12090−12101.
(30) Godfrin, C.; Ferhat, A.; Ballou, R.; Klyatskaya, S.; Ruben, M.; Wernsdorfer, W.; Balestro, F. Operating Quantum States in Single Magnetic Molecules: Implementation of Grover's Quantum Algorithm. *Phys. Rev. Lett.* **2017**, *119*, 187702.
(31) Aguilà, D.; Barrios, L. A.; Velasco, V.; Roubeau, O.; Repollés, A.; Alonso, P. J.; Sesé, J.; Teat, S. J.; Luis, F.; Aromí, G. Heterodimetallic [LnLn′] Lanthanide Complexes: Toward a Chemical Design of Two-Qubit Molecular Spin Quantum Gates. *J. Am. Chem. Soc.* **2014**, *136*, 14215−14222.
(32) Leuenberger, M. N.; Loss, D. Quantum Computing in Molecular Magnets. *Nature* **2001**, *410*, 789−793.
(33) Moreno-Pineda, E.; Klyatskaya, S.; Du, P.; Damjanović, M.; Taran, G.; Wernsdorfer, W.; Ruben, M. Observation of Cooperative Electronic Quantum Tunneling: Increasing Accessible Nuclear States in a Molecular Qudit. *Inorg. Chem.* **2018**, *57*, 9873−9879.
(34) Schlegel, C.; van Slageren, J.; Manoli, M.; Brechin, E. K.; Dressel, M. Direct Observation of Quantum Coherence in Single-Molecule Magnets. *Phys. Rev. Lett.* **2008**, *101*, 147203.
(35) Kumar, K. S.; Serrano, D.; Nonat, A. M.; Heinrich, B.; Karmazin, L.; Charbonnière, L. J.; Goldner, P.; Ruben, M. Optical Spin-State Polarization in a Binuclear Europium Complex towards Molecule-Based Coherent Light-Spin Interfaces. *Nat. Commun.* **2021**, *12*, 2152.
(36) Serrano, D.; Kuppusamy, S. K.; Heinrich, B.; Fuhr, O.; Hunger, D.; Ruben, M.; Goldner, P. Ultra-Narrow Optical Linewidths in Rare-Earth Molecular Crystals. *Nature* **2022**, *603*, 241−246.
(37) Binnemans, K. Interpretation of Europium(III) Spectra. *Coord. Chem. Rev.* **2015**, *295*, 1−45.
(38) Pedersen, K. S.; Ungur, L.; Sigrist, M.; Sundt, A.; Schau-Magnussen, M.; Vieru, V.; Mutka, H.; Rols, S.; Weihe, H.; Waldmann, O.; et al. Modifying the Properties of 4f Single-Ion Magnets by Peripheral Ligand Functionalisation. *Chem. Sci.* **2014**, *5*, 1650−1660.
(39) Bernhardt, P. V.; Flanagan, B. M.; Riley, M. J. Completion of the isomorphous Ln(trensal) series. *Aust. J. Chem.* **2001**, *54*, 229.
(40) Alvarez, S. Continuous Shape Measures Study of the Coordination Spheres of Actinide Complexes − Part 1: Low Coordination Numbers. *Eur. J. Inorg. Chem.* **2021**, *2021*, 3632−3647.
(41) Flanagan, B. M.; Bernhardt, P. V.; Krausz, E. R.; Lüthi, S. R.; Riley, M. J. A Ligand-Field Analysis of the Trensal (H_3Trensal = 2,2',2'' -Tris(Salicylideneimino)Triethylamine) Ligand. An Application of the Angular Overlap Model to Lanthanides. *Inorg. Chem.* **2002**, *41*, 5024−5033.
(42) Könz, F.; Sun, Y.; Thiel, C. W.; Cone, R. L.; Equall, R. W.; Hutcheson, R. L.; Macfarlane, R. M. Temperature and Concentration Dependence of Optical Dephasing, Spectral-Hole Lifetime, and Anisotropic Absorption in Eu^{3+}:Y_2SiO_5. *Phys. Rev. B: Condens. Matter Mater. Phys.* **2003**, *68*, 085109.
(43) Kreidt, E.; Kruck, C.; Seitz, M. Nonradiative Deactivation of Lanthanoid Luminescence by Multiphonon Relaxation in Molecular Complexes. *Handbook on the Physics and Chemistry of Rare Earths*; Elsevier: Radarweg 29, PO Box 211, 1000 AE Amsterdam, The Netherlands, 2018; Vol. *53*, pp 35−79.
(44) Beeby, A.; Clarkson, I. M.; Dickins, R. S.; Faulkner, S.; Parker, D.; Royle, L.; de Sousa, A. S.; Williams, J. A. G.; Woods, M. Non-Radiative Deactivation of the Excited States of Europium, Terbium and Ytterbium Complexes by Proximate Energy-Matched OH, NH and CH Oscillators: An Improved Luminescence Method for Establishing Solution Hydration States. *J. Chem. Soc., Perkin Trans. 2* **1999**, 493−504.
(45) Tanner, P. A. Some Misconceptions Concerning the Electronic Spectra of Tri-Positive Europium and Cerium. *Chem. Soc. Rev.* **2013**, *42*, 5090.
(46) Yanagisawa, K.; Nakanishi, T.; Kitagawa, Y.; Seki, T.; Akama, T.; Kobayashi, M.; Taketsugu, T.; Ito, H.; Fushimi, K.; Hasegawa, Y. Seven-Coordinate Luminophores: Brilliant Luminescence of Lanthanide Complexes with C_{3v} Geometrical Structures. *Eur. J. Inorg. Chem.* **2015**, *2015*, 4769−4774.
(47) Yanagisawa, K.; Kitagawa, Y.; Nakanishi, T.; Akama, T.; Kobayashi, M.; Seki, T.; Fushimi, K.; Ito, H.; Taketsugu, T.; Hasegawa, Y. Enhanced Luminescence of Asymmetrical Seven-Coordinate Eu III Complexes Including LMCT Perturbation. *Eur. J. Inorg. Chem.* **2017**, *2017*, 3843−3848.
(48) Ahlefeldt, R. L.; Manson, N. B.; Sellars, M. J. Optical Lifetime and Linewidth Studies of the Transition in : A Potential Material for Quantum Memory Applications. *J. Lumin.* **2013**, *133*, 152−156.
(49) Binnemans, K.; Görller-Walrand, C. Crystal Field Analysis of EuCl3.6H2O. *J. Alloys Compd.* **1997**, *250*, 326−331.
(50) Shelby, R. M.; Macfarlane, R. M. Frequency-Dependent Optical Dephasing in the Stoichiometric Material EuP5O14. *Phys. Rev. Lett.* **1980**, *45*, 1098−1101.
(51) Ortu, A.; Rakonjac, J. V.; Holzäpfel, A.; Seri, A.; Grandi, S.; Mazzera, M.; de Riedmatten, H.; Afzelius, M. Multimode Capacity of Atomic-Frequency Comb Quantum Memories. *Quantum Sci. Technol.* **2022**, *7*, 035024.
(52) Tanaka, M.; Kushida, T. Effects of Static Crystal Field on the Homogeneous Width of the 5D0− 7F0 Line of Eu3+ and Sm2+ in Solids. *Phys. Rev. B: Condens. Matter Mater. Phys.* **1995**, *52*, 4171−4178.
(53) Serrano, D.; Karlsson, J.; Fossati, A.; Ferrier, A.; Goldner, P. All-Optical Control of Long-Lived Nuclear Spins in Rare-Earth Doped Nanoparticles. *Nat. Commun.* **2018**, *9*, 2127.
(54) Pettit, R. M.; Farshi, F. H.; Sullivan, S. E.; Osorio, Á. V.; Singh, M. K. A Perspective on the Pathway to a Scalable Quantum Internet Using Rare-Earth Ions. **2023**, arXiv:2304.07272.
(55) Mor, O. E.; Ohana, T.; Borne, A.; Diskin-Posner, Y.; Asher, M.; Yaffe, O.; Shanzer, A.; Dayan, B. Tapered Optical Fibers Coated with Rare-Earth Complexes for Quantum Applications. *ACS Photonics* **2022**, *9*, 2676−2682.
(56) Shin, A. J.; Zhao, C.; Shen, Y.; Dickerson, C. E.; Li, B. Y.; Bím, D.; Atallah, T. L.; Oyala, P. H.; Alson, L. K.; Alexandrova, A. N.; et al. Toward Liquid Cell Quantum Sensing: Ytterbium Complexes with Ultra-Narrow Absorption. **2022**, ChemRxiv:2022-vg4jr.